FRAGMENTATION EVENT DEBRIS FIELD EVOLUTION USING 3D VOLUMETRIC RISK ASSESSMENT

David A. Vallado[1], Daniel L. Oltrogge[2]

[1] Senior Research Astrodynamicist, Center for Space Standards and Innovation, Analytical Graphics Inc., 7150 Campus Drive, Suite 260, Colorado Springs, Colorado, 80920-6522. dvallado@agi.com

[2] SDC Program Manager & Senior Research Astrodynamicist, Center for Space Standards and Innovation, Analytical Graphics Inc., 7150 Campus Drive, Suite 260, Colorado Springs, Colorado, 80920-6522. doltrogge@agi.com

ABSTRACT

The evolution of the debris field generated by an on-orbit explosion or collision fragmentation event is of critical concern to space operators and SSA organizations. The debris field can be initially generated by combining one of the available breakup models containing imparted velocity and fragment size probability density functions (PDFs), with efficient lambert solutions and 3D time-based PDF mappings. Previous relevant techniques for simulating this are examined. Existing two-dimensional debris field evolution and dynamics approaches are extended to three dimensions. To do this, the full set of possible lambert solutions is employed, to include multi-revolution solutions. The resulting PDF distributions are dynamically shown in three dimensions for various sample collision and explosion cases, in several important orbital classes. Finally, we evaluate the active satellites potentially put at risk by the evolving debris cloud.

1. INTRODUCTION

The evolution of debris patterns resulting from an on-orbit fragmentation event (such as a collision, explosion or intercept) are of increasing interest and importance as the number of satellites increase. Satellite operators need actionable and well-founded Space Situational Awareness (SSA) in the event that such a fragmentation occurs. Currently, insufficient research and modelling have been done in this area to provide such actionable SSA. We review the relevant works in this area, with a particular emphasis on what assumptions researchers have made regarding the dimensionality of the examined problem set (two-dimensional, 2D, vs three dimensional, 3D), what initial velocity distributions or percentiles are adopted, and the resulting net effect on collisions probability.

Two types of debris fragmentation simulations are typically conducted: (a) Generation of a representative debris field and its evolution over time; and (b) Assessment of where fragments could possibly go and the associated risk that those fragments will actually be there.

When conducting the first type of simulation, it is important to conserve basic physical properties, including mass, linear momentum and kinetic energy. As has been noted previously (Finkleman & Oltrogge, 2008), the NASA Standard Breakup Model fails to conserve any of these parameters (violating equations (1) below for conservation of mass, momentum, and energy (Chobotov 1988). As a practical matter, conservation of kinetic energy is relatively easy because so much of a collision's energy is lost to rotational energy, particle separation, heat and light.

$$\begin{aligned}
&(m_1+m_2)_{before} = (m_1+m_2)_{after} \\
&m_1\vec{v}_1 + m_2\vec{v}_2 = 0 \\
&\frac{m_1 v_1^2}{2} + \frac{m_2 v_2^2}{2} = \frac{m_1 v_1^2}{2} + \frac{m_2 v_2^2}{2} \\
&\qquad + \frac{1}{2} \quad p_1\left(\vec{v}_1\cdot\vec{v}_1\right)^2 d^3 v_1 \\
&\qquad + \frac{1}{2} \quad p_2\left(\vec{v}_2\cdot\vec{v}_2\right)^2 d^3 v_2 + Q_{lo.}
\end{aligned} \tag{1}$$

Our focus will instead be on the second type of analysis, where we wish to ascertain where fragments from a collision or explosion may possibly go, and what is the overall likelihood that they went to a place (or orbit) of interest. In this second type of analysis, whether basic physical properties such as mass, linear momentum and kinetic energy are conserved is of little concern. Rather, the focus on this type of analysis needs to be to ensure that the relative velocities and their associated probability density functions are as representative and actionable as possible. This is difficult to achieve, of course, because so much of that depends upon the initial conditions of the colliding or exploding object(s), their materials, etc. For this paper, the considered best low-fidelity models were adopted, but we look forward to employing higher-fidelity breakup models in the future as well.

A note on our terminology. One may consider the portions of satellites involved in a collision as being either "non-involved" or "involved." ***Involved*** portions represent the portion of the satellite which directly impacts the other space object, while ***non-involved*** fragments are "external" features such as solar cells, antennae, etc. that may not be directly involved in the collision but may "inherit" some of the collision's kinetic energy and themselves fragment. The involved and non-involved classes of fragments likely have different relative velocity distributions. While breakup models are most relevant to involved portions of the spacecraft, the non-involved portions may be subject to subsequent fracturing and other phenomena. Accordingly, the 1Earth DEBBIE (Oltrogge, 2008) implementation of the NASA EVOLVE standard breakup model treats the involved and non-involved portions of each satellite (four categories, as shown in the figure below) as separate mass groupings, with the imparted relative velocities for each of the four categories being potentially different and each centered about in independent center-of-mass velocity vector (depending on user assumptions regarding any momentum transfer that might occur).

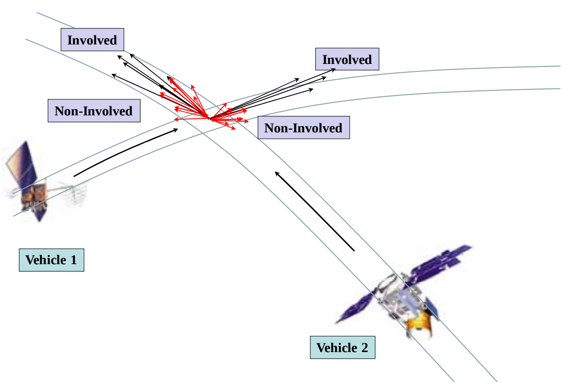

Figure 1: Collision Geometry. This figure shows a notional collision between two satellites. Involved portions of the satellites represent the collision "overlap" between the two satellites, while non-involved objects are the parts that don't overlap. Depending on the specific collision case, non-involved portions may be less massive and/or smaller components, such as solar cell arrays, antennae, etc.

2. HISTORICAL ANALYSES

Analyses have taken many forms over the years. An initial depiction used the Gabbard (Gabbard 1981) plot (apogee and perigee altitudes vs orbital period). While good for early analyses, the static depiction of a 2D orbital plane didn't capture the full range of motion expected from an arbitrary collision.

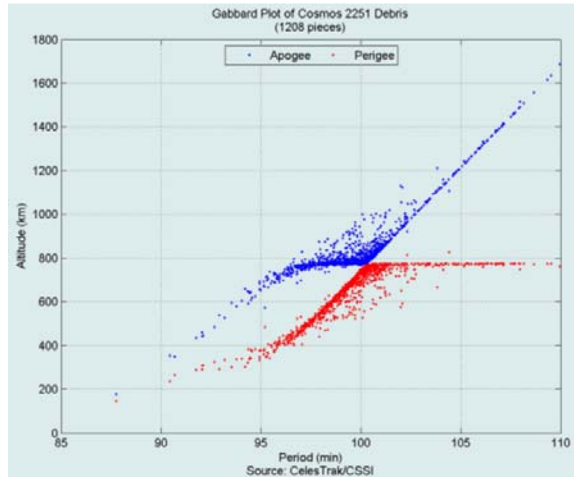

Figure 2: Gabbard Depiction. This figure shows the apogee and perigee values vs the period for particles of a collision. The two "lines" show the general direction of the two objects before the collision. (Figure from Celestrak)

Hujsak (1991) developed a nonlinear relative motion model to avoid the uncertainties in a simple linear fragmentation model, or an approach that does not conserve mass, momentum, or energy. He found that "average particle density can seriously misrepresent actual particle density." Hujsak also conceived the idea of employing Lambert's Solution to determine where debris fragments could go, but computational capabilities were insufficient at that time to follow that thread. Hujsak's work was partial inspiration for Healy (2016) and for our concept.

McKennon-Kelly (2015) examined various approaches used by Aerospace to analyze debris events. Runtime was an important consideration and resulted in the development of toroidal regions that permitted faster computational times.

Healy (2016) provides a concise summary of additional techniques and approaches, ultimately settling on a transformation of variables approach using the Lambert algorithm. He introduces the concept of cloud dynamics and the evolution of a density distribution over time, as opposed to point dynamics which is the usual case for astrodynamics/celestial mechanics. The transformation of variables finds the set of final position /velocity vectors based on an initial position and velocity distribution. This can be applied to any initial velocity distribution. Healy (2016) limited the dimensions of the analysis space and rotated the Lambert solutions to find a 3D solution containing the collision. The essence of his approach is as follows:

The transformation of variables finds a normalized number density at any point in space. He uses reciprocal distance ($1/km^3$) – essentially a probability density function. Two things are needed:

1. The determinant of the Jacobian at each of these final position points (solving Lambert's problem)
2. The final position points from an initial position and velocity distribution (propagation)

The advantage of this approach is that one can calculate a new set of final position points from a different initial velocity distribution from the existing distribution map, rather than from scratch, significantly enhancing the performance.

3. PRESENT SCOPE

We build on Healy's idea and extend 2D debris field evolution and dynamics approaches to three dimensions. While this extension is significantly more computationally expensive, careful attention to programming, efficient algorithms, and efficient gridding techniques proved useful to streamline the analysis and yield acceptable run times. Our approach uses 3D equal angles grid at concentric shells of altitude to represent, at any given time of interest, all possible locations that fragments could go; these grid points are then evaluated using the full complement of possible Lambert solutions (including multi-revolution solutions) to determine what Δv would be required in order for an fragment to reach a particular grid point in the prescribed time. This resulting Δv is then compared with the normalized PDF distribution to ascertain the likelihood that a fragment would actually have been imparted. Finally, we evaluate the active satellites potentially put at risk by the evolving debris cloud.

While building on previous efforts, we employed new techniques to provide greater flexibility and hopefully achieve greater realism in the resulting 3D debris risk representation. The initial debris generation is combined with fast gridding techniques to store all the data, and produce 2D and 3D visualization of the results. Overall goals of this new approach are:

- Fast, robust execution processing
- Incorporate fragmentation dispersal effect
- Employ full Δv -vs-L_c PDFs
    - Avoid arbitrary selection of "outer skin" (e.g. 95th percentile) Δv
    - Based on best breakup model-derived Δv predictions
- Realistic probability-based debris risk evolution and dispersal
    - Use an efficient gridding system
    - Employ full complement of Lambert solutions
    - Suitable for collision and explosion fragmentation events
- Generate dynamic 2D portrayals of fragmentation dispersal
- Generate dynamic 3D volumetric portrayals of fragmentation dispersal and spacecraft collision risk
    - Facilitate further satellite risk analyses by combining object dispersion and collision risk to spacecraft

4. DEBRIS ENVIRONMENT

Debris, from natural causes and from explosions and collisions, is increasing. As of April 2017, there are about 4400 payloads on orbit, with almost 14000 debris objects.

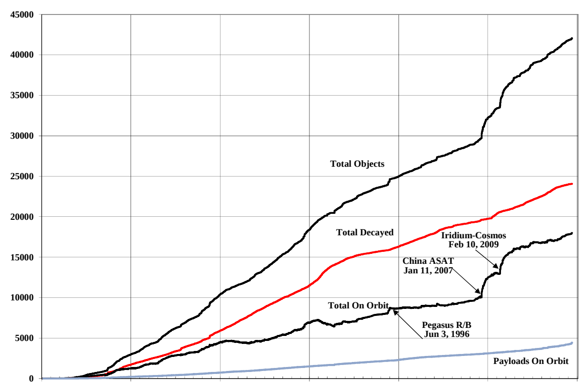

Figure 3: Space Object Growth. This figure shows the progression of space objects over time. Debris events can generate significant debris. Payloads represent less than 30% of the entire catalog today (as of April 2017).

The first on-orbit fragmentation occurred 29 Jun 1961 with the Ablestar Stage (Johnson, 2008). The number of breakups are shown below.

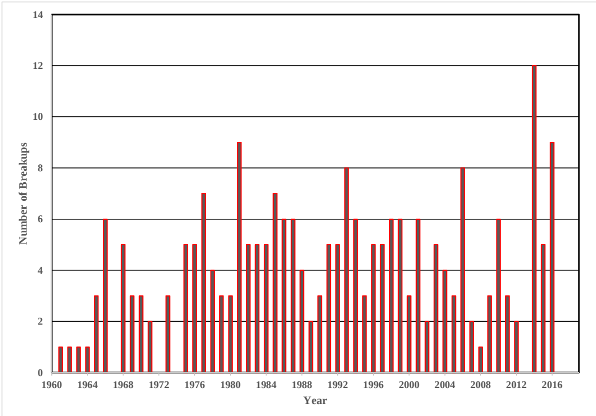

Figure 4: Space Object Breakups. There have not been a lot of breakups, but some of the events have produced very large numbers of debris objects. (Figure updated from Johnson 2008)

While there have been relatively few objects to breakup, the number of fragments is large. Fortunately, natural decay removes many of the objects over time.

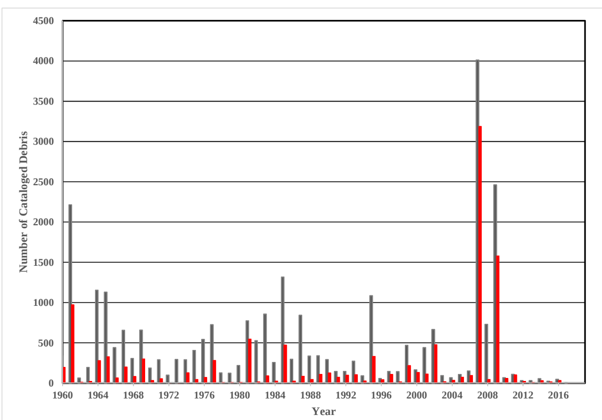

Figure 5: Debris Distribution. This figure shows the number of debris objects cataloged by the U.S. Air Force. The black column is the current number of fragments and the red column is the current number (as of April 2017). Note these include collision/explosions as well as incidental debris resulting from launches. Note the rapid decay of many particles in some situations.

5. MODELLING THE DISTRIBUTIONS

A key in any simulation is the development of the initial velocity distributions. To date, the most common assumption we've seen researchers use is to adopt a specific initial relative velocity (e.g. a fixed value or at best an adopted percentile of the Δv PDF. Generally, it is acceptable to assume an omnidirectional spread of particles about the center-of-mass velocity vector (typically aligned with the directions of the initial orbital velocities for both colliding objects).

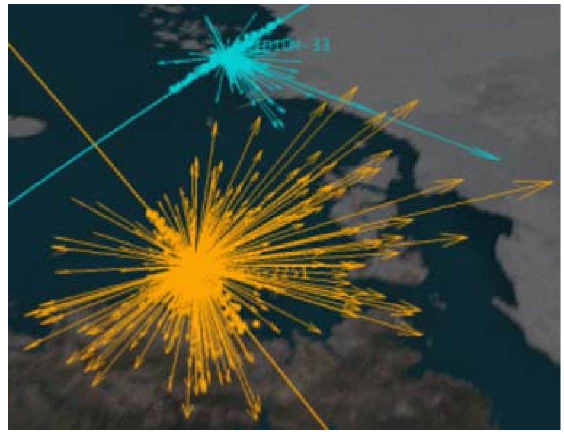

Figure 6: Initial Velocity Distribution. This figure shows the fragmentation-induced relative velocities derived from TLEs released after the Cosmos-Iridium collision in 2009 (Feb 10, 2009 16:55:59.806284 UTC, v_{rel} = 11.647263 km/s). Note that only larger objects were *successfully tracked* and depicted here. Also note that the initial dispersions are moved slightly in time from the collision to show the differences in the two distributions of objects. (Figure from CelesTrak)

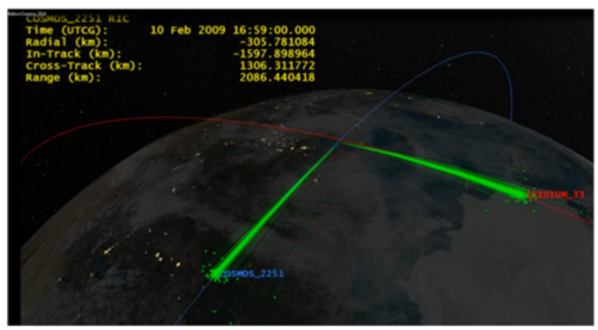

Figure 7: Initial Velocity Distribution. This figure shows the *simulated* DEBBIE equivalent breakup scenario corresponding to the initial conditions for the Iridium/Cosmos collision of 2009. Note the blunt leading edge of the fragments at the leading edge of the debris field, as well as the spread of objects far from the original orbital path.

Using a Lambert-based approach to identify all possible paths for a debris fragment to get from the fragmentation event to any 3D location of interest is advantageous because it will capture all events not found from the initial "measured" or observed distribution, or from simulations that generate a representative debris field (without generating the overall encompassing envelop within which that debris could possibly be located).

To evaluate the debris initial velocity distributions the NASA EVOLVE 4.0 debris breakup model (Johnson et al. 2001) was used along with ESA's suggested associated modifications, inputting the size (a general description of the area, ***characteristic length*** is used in m, which is 1/3 of the sum of the largest dimensions in each orthogonal direction 1/3(a + b + c)), collision velocity, area-to-mass ratios, and fragment masses and population. 1Earth Research implemented this these breakup models (and others) to allow simple specification of the various inputs to generate sophisticated, representative discrete fragmentation scenarios. DEBBIE (Oltrogge, 2008) performs this initial velocity distribution calculation.

Size is determined by Johnson et al. (2001) assuming the debris is spherical with the density of aluminum below 1 cm, and a density of $\rho(d) = 92.937(d)^{-0.74}$ for objects larger than 1 cm. He differentiates between explosions and collisions because the size and number of particles differs between each event. For explosions, larger objects are created.

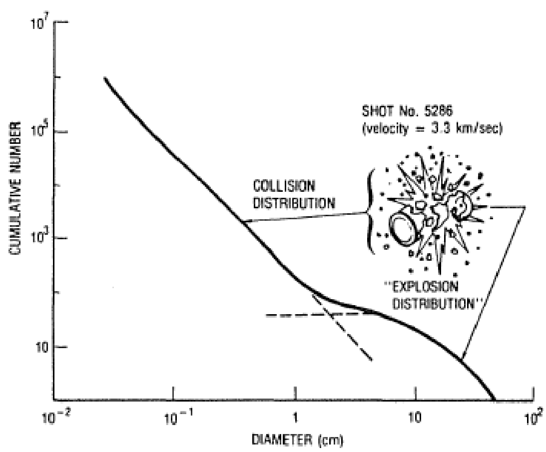

Figure 8: Initial Velocity Distribution. The number of fragments from a collision and an explosion differ in terms of size and number. (Figure from Chobotov, 1988:75)

For explosions, the number of particles larger than a particular size (L_c) is defined to be $N(L_c) = S\ 6\ L_c^{-1.6}$ where S is a scaling parameter to account for the size of the objects involved. For collisions, the number of particles larger than a particular size (L_c) is $N(L_c) = 0.1\ M^{0.75}\ L_c^{-1.71}$ where M is the mass.

6. Sample Δv distributions

Next, we examine resulting sample Δv PDFs for several sample collision cases. Note that we employ the 3D Plot.ly depiction (https://plot.ly/) to provide a convenient platform to dynamically move the figure between two and three dimensions. As can be seen from the figures below, Δv statistics can be derived from the Δv PDFs as a $f(L_c)$.

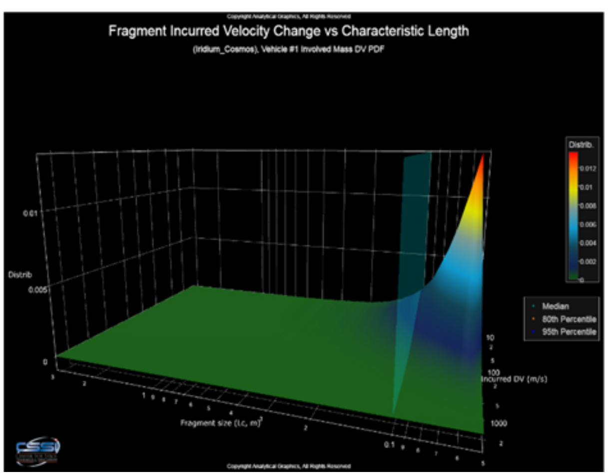

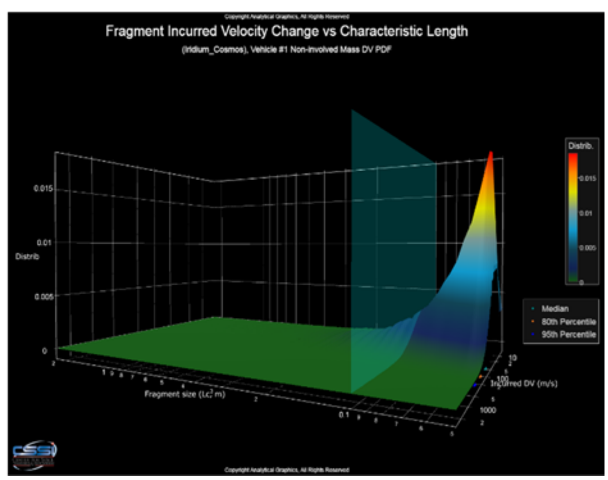

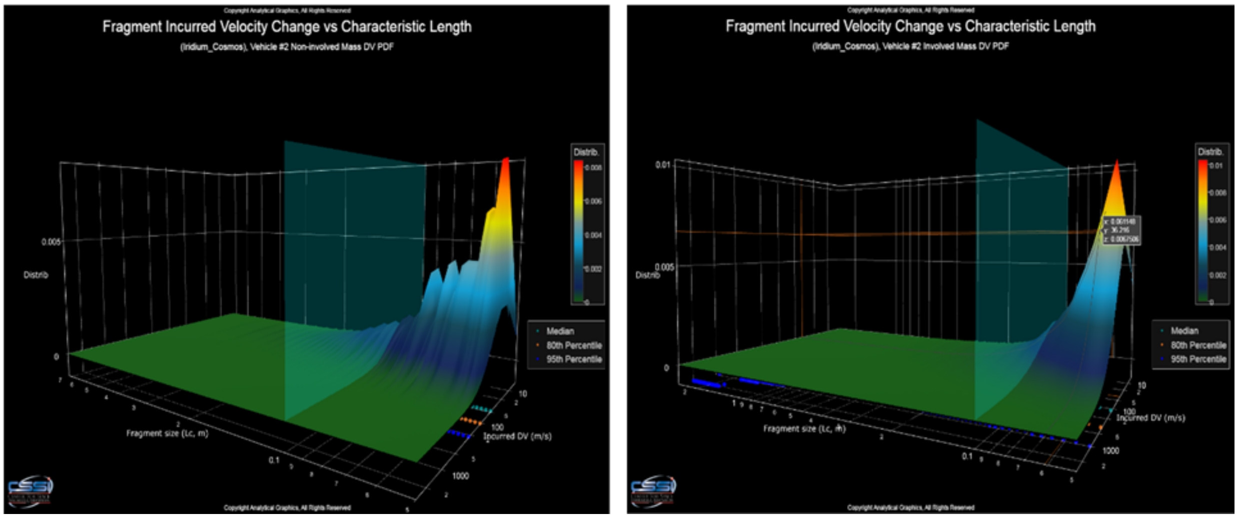

Figures 9: Characteristic Length vs Fragmentation Δv and Distribution. The involved and non-involved distributions (left and right respectively) are shown for both vehicles.

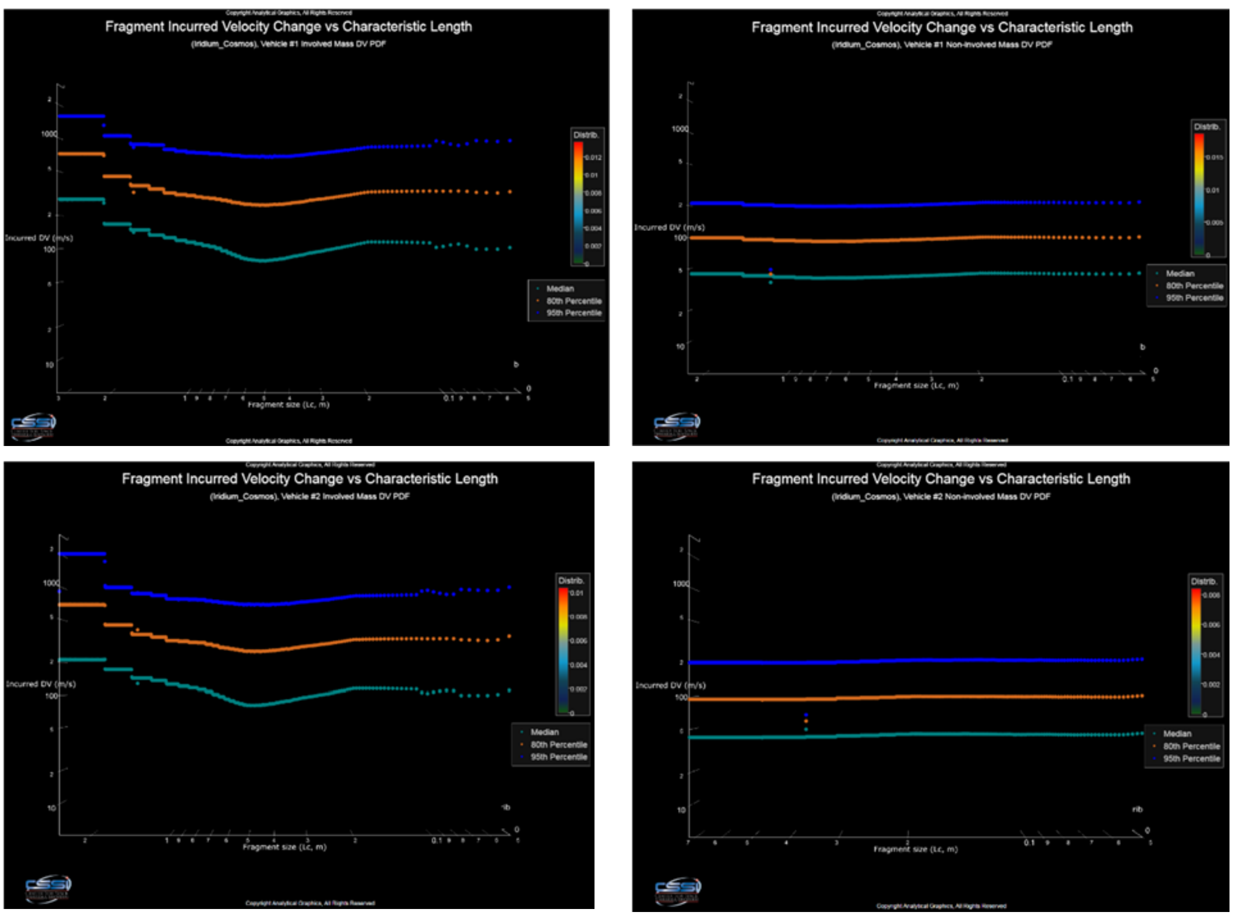

Figures 10: Characteristic Length vs Fragmentation Δv. The involved and non-involved distributions (left and right respectively) are shown for both vehicles.

7. MODELLING THE FRAGMENT LOCATIONS

Our overall goal is to systematically/parametrically sample all locations in three-dimensional space to quickly determine all possible trajectories (Lambert, Vallado 2013:492) that can travel in a specified Time of Flight (ToF) between the initial fragmentation location and the prospective final satellite spatial positions. The resulting Δv s each of these trajectories require can then be compared to the Δv PDFs for a characteristic length (L_c) of interest to determine what the likelihood of a debris fragment receiving that Δv.

We chose to represent our locations using concentric shells of equal-angle grid points. These points are stored in a fast and efficient framework for fast use and ease of interpolation (AstroHD, Oltrogge AIAA 2008-7065). Use of such a grid reduces data analysis (CPU processing), storage and networking requirements by 40%. Oltrogge (2008) designed this approach around an icosahedron shape (a regular polyhedron). The basic shape is a subdivided icosahedron framework, where all of the subdivided faces are very nearly equilateral triangles.

Oltrogge's approach to constructing an equal-angles framework based on subdivision of an icosahedron originally drew upon the work of Chobotov et al. (1988). Each face of an icosahedron is an equilateral triangle, so all distances between the vertices are the same. The distance of each vertex to the geometric center is also the same. The basic parameter is the golden ratio (φ). To create all the vertices on a unit sphere, Chobotov define $s\varphi$ and $t\varphi$ as follows.

$$\varphi = \frac{1+\sqrt{5}}{2} \qquad s\varphi = \frac{\sqrt{5-\sqrt{5}}}{10} \qquad t\varphi = \frac{\sqrt{5+\sqrt{5}}}{10} \tag{2}$$

Chobotov then generated all vertices by taking all permutations for all the vertexes; shown below are three vectors for which each variable takes on ± signs to find all 12.

$$[s\varphi\ t\varphi\ 0] \text{ and } [0\ s\varphi\ t\varphi] \text{ and } [t\varphi\ 0\ s\varphi]$$

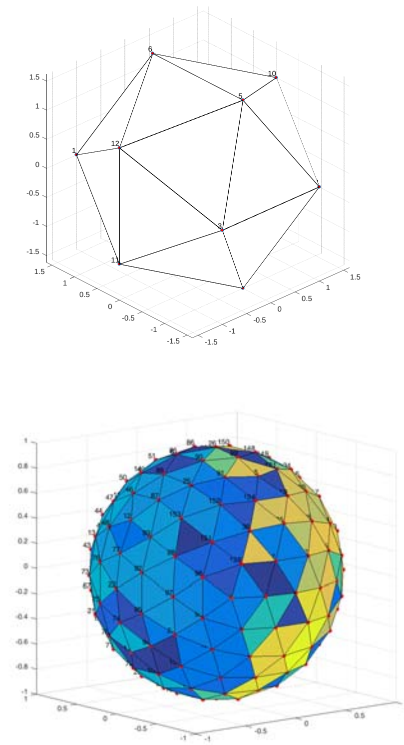

Figure 11: Icosahedron Geometry. This figure shows a standard icosahedron on the top, and a twice subdivided version on the bottom (F = 320, V = 162, E = 480). Notice that the points for the subdivided object are placed a sphere so all vertices are at the same distance from the origin. Also, the points are numbered to indicate "an" approach in numbering each vertex. This becomes important when finding regions for calculation.

As we subdivide each primary triangle of the icosahedron, the number of vertices and points increase rapidly (N is the number of subdivisions along an icosahedron primary vertex as shown in the figure below).

$$N_{vertices} = 12 + 10[2(\sum_{i=2}^{N+1} i) - 3N - 1] \tag{3}$$

$$Angular\ Separation = [\frac{tan^{(-1)}2}{N}]$$

The number of AstroHD grid points and resulting angular separation are shown in Table 1.

Table 1: Number of equal-angles grid points and corresponding angular separation as f (N)

N	$N_{vertices}$	Angular Separation (deg)	Equivalent # Rectangular Grid Points
1	12	63.4349488229220	16
12	1,442	5.28624573524350	2,315
32	10,242	1.98234215071631	16,200
64	40,962	0.99117107535816	64,800
127	161,292	0.49948778600726	259,200
254	645,162	0.24974389300363	1,036,800
318	1,011,242	0.19948097114126	1,620,000
635	4,032,252	0.09989755720145	6,480,000
1269	16,103,612	0.04998813934036	25,920,000
6344	402,463,362	0.00999920378672	648,000,000

Each face is easily subdivided using the same icosahedron approach. In the most general sense, all orbital altitudes could be examined. We selected an AstroHD subdivision of N=127, corresponding to 161,292 vertices separated by ≈ 0.5° (≈ 61 km apart at 700 km altitude), to represent all potential final locations at each of the various orbital altitudes. Ultimately, we arrived at a solution where the various concentric equal-angles spherical shells were 50 km apart, roughly corresponding to the AstroHD grid point distance separation of 61 km.

Increasing the number of subdivisions of each Icosahedron face and employing great circles to maximize the uniformity of the grid yields the fine mesh grid as shown in the figure below. Note that although a slight pixel aliasing exists when viewing the grid on a computer, the grid point separations are quite uniform.

There are several challenges to programming the AstroHD approach. Notice that the order of points is important! First is maintaining book-keeping of vertex numbering so fast retrieval is possible. Next is a fast algorithm to retrieve the pre-computed values. Finally, efficient interpolation techniques are required to find values between existing grid points.

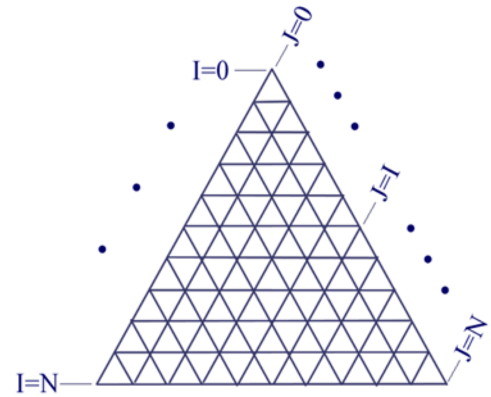

Figure 12: Numbering Scheme. AstroHD indexing scheme for the icosahedron shape

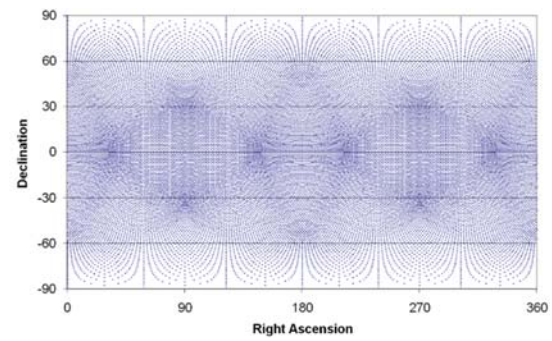

Figure 13: Icosahedron Mesh Grid Plot. This figure shows the distribution of the mesh grid in right ascension-declination space.

8. LAMBERT SOLUTIONS

There are numerous implementations of the Lambert routine where two position vectors ($\vec{r}_1, \vec{r}_2$) and the time of flight are known. Vallado (2013:467 Sec 7.6) discusses several approaches for solution. We'll see later that using Lambert lets us find one orbital solution at the final time, and then screening the lower altitudes using the single solution. This has computational benefits over propagating each fragment independently. We found the approach of Nitin and Russel (2013) to be useful. They transform the usual universal variable and define a parameter k in terms of the eccentric anomaly.

$$\cos(\Delta E) = k^2 - 1 \quad (4)$$

Defining several parameters including the direction of motion ($d = \pm 1$ for long and short way trajectories), one can find a time of flight equation as follows. The n_{rev} term enables multiple revolutions in the solutions.

$$
\begin{aligned}
&\tau = d\,\frac{\sqrt{r_1 r_2 (1+\cos(\Delta\theta))}}{r_1 + r_2} \\
&q = 1 - sign(k)\pi + sign(k)\cos^{-1}(k^2 - 1) \\
&\qquad + 2\pi n_{rev} \\
&s = \sqrt{\frac{r_1 + r_2}{\mu}} \\
&m = 2 - k^2 \\
&w = \frac{q}{\sqrt{m^3}} - \frac{k}{m} \\
&tof = s\sqrt{1 - k\tau}(\tau + (1 - k\tau)w)
\end{aligned}
\tag{5}
$$

The literature generally discusses the short way and long way to the target. Note there also exist direct and retrograde solutions, each of which has short way and long way trajectories to the target, shown in Figure 11 below.

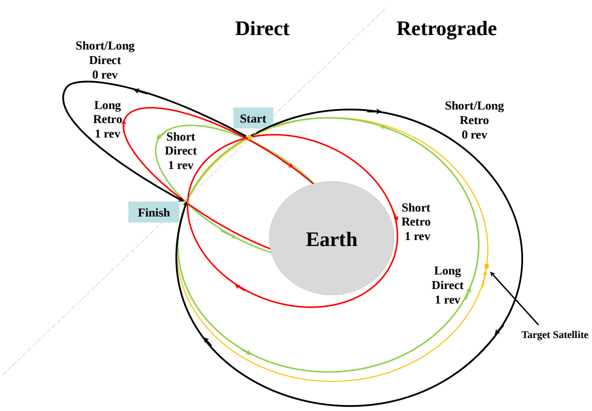

Figure 14: Lambert Transfer Geometry. This figure shows the various transfers for 0-revolution, and 1-revolution cases. Some trajectories impact the Earth during transfer.

Some options to speed up. First, eliminate cases that are within a volume that must go through the Earth.

A simplistic time filter was applied to reduce cases that could not achieve a given location in the data grid. If the time of flight was greater than the magnitude of the relative range vector divided by the magnitude of the initial Δv component in the relative range direction, transfers were calculated. This saved a great deal of computational time.

Next, ambiguity arises in Lambert for cases with transfers of 180° and 360° (plus multiples thereof). We constrained the velocity change to take place in the direction of the initial orbital velocity. The angle of rotation is found from the dot product of the angular momentum of the fragment and the fragment using the Lambert velocity. The Lambert velocity is then rotated to be in the direction of the initial fragment.

9. DEBRIS EVOLUTION

A simplistic convention to illustrate the debris spread is to examine a tube- or ring-like structure surrounding the original orbits. This has gradually been replaced by more sophisticated techniques.

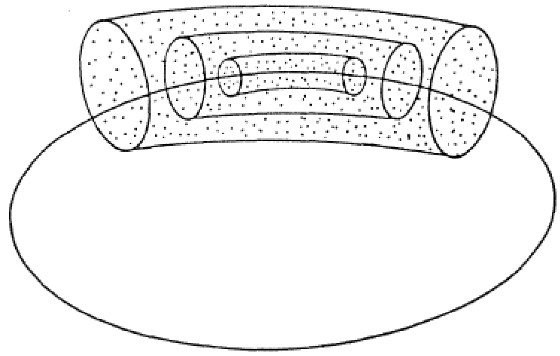

Figure 15: Simplistic Geometry. This figure shows an overly-simplistic view of the region where debris could be located. (Figure from Chobotov 1988:113)

The NASA EVOLVE 4.0 software (Johnson et al. 2001) contains the NASA Standard Breakup Model, which overlays multiple distributions to estimate fragmentation velocities and area-to-mass ratios as a function of fragment size. The model establishes categories smaller than 8 cm, larger than 11 cm, and larger than 35 cm. There is a bridge function for sizes between 8 and 11 cm. Again distinguishing between explosions and collisions,

$$
G(x) = \frac{1}{2\sqrt{\pi\sigma^2}}\exp[-\frac{(\log_{10}(\Delta v) - \mu^{exp})^2}{2\sigma^2}] \tag{6}
$$

where Δv is the magnitude of the change in velocity, $\chi = \log_{10}(A/m)$, and σ is 0.4. For explosions, $\mu^{exp} = 0.2\,\chi + 1.85$, and for collisions, $\mu^{coll} = 0.9\,\chi + 2.9$. We note that the debris model is intended for hypervelocity events (faster than the speed of sound in the medium).

While the LEGEND software release updated NASA's debris analysis software offerings at several levels, the basic NASA Standard Breakup Model that LEGEND incorporates remains the same as was in

LEGEND's precursor (EVOLVE) software. This model is included in its full detail in the DEBBIE program, with additional capability to use ESA's suggested small particle improvements. The LEGEND model is identical to the previously released EVOLVE 4.0 model. NASA has done a comparison between the observed fragmentation from the Iridium/Cosmos collision and LEGEND, as well as the Chinese ASAT test. The agreement was pretty good, but not in all respects.

10. PROCESS

Our overall goal is to produce a full 3D representation of the resulting distribution of pieces over time. The overall process combines the approaches introduced earlier. It looks like this.

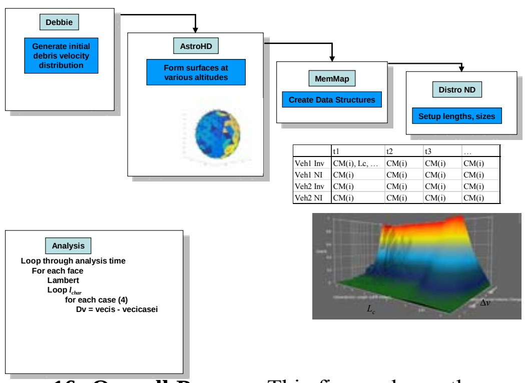

Figure 16: Overall Process. This figure shows the overall processing. Several computer programs are combined to arrive at the final solution.

An analysis using the Volumetric Encounters method (Alfano and Oltrogge 2015) indicates the rate at which collisions expected. The "focus is on determining the time durations and frequencies where an overlap within a prescribed ellipsoidal encounter volume could occur between two satellites randomly positioned in their orbits. They also determined the average aggregate number of probable encounters over a period of time to produce a reasonable expectation of proximity warnings (not necessarily collisions) per day or week an operator might expect." Houlton and Oltrogge (2014) also characterized the spatial density in 3D (both its time evolution and a static depiction). These prior tools and approaches complement this paper's functionality quite well, in that the tools can quantify the likelihood of collision for a satellite of interest, and then this paper's tool (DREAD) can quantify risk to other operator spacecraft in the unfortunate circumstance that such a collision occurs.

11. RESULTS

We chose two conjunctions to illustrate the approach. The Iridium-33/Cosmos-2251 (February 10, 2009 16:55:59.806284 UTC, v_{rel} = 11.647 263 km/s) collision is useful because it generated a lot of debris that is still in orbit today. A hypothetical low velocity GEO impact (v_{rel} = 0.805 515 km/s) allowed us to visualize a different scenario based on some limited observations and papers by (Hanada, 2000). To ensure we had a correct solution, we examined 2D, then 3D slices, and finally full 3D simulations. First examine a 2D plot of the debris generated. Using an inertial right ascension – declination space, the colored points in the 2D plots below denote the likelihood, aggregated across all four Δv PDFs (S/C #1 Involved, S/C #1 Non-involved, S/C #2 Involved, S/C #2 Non-involved), that a fragment will acquire a fragmentation-imparted Δv necessary for the fragment to travel from the fragmentation location to any point on the equal-angles grid in the parametrically-sampled Lambert Time of Flight. The legend matching the colors for these points is provided at the right.

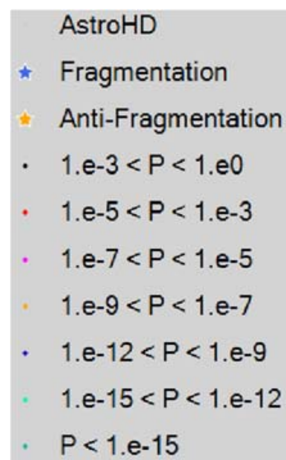

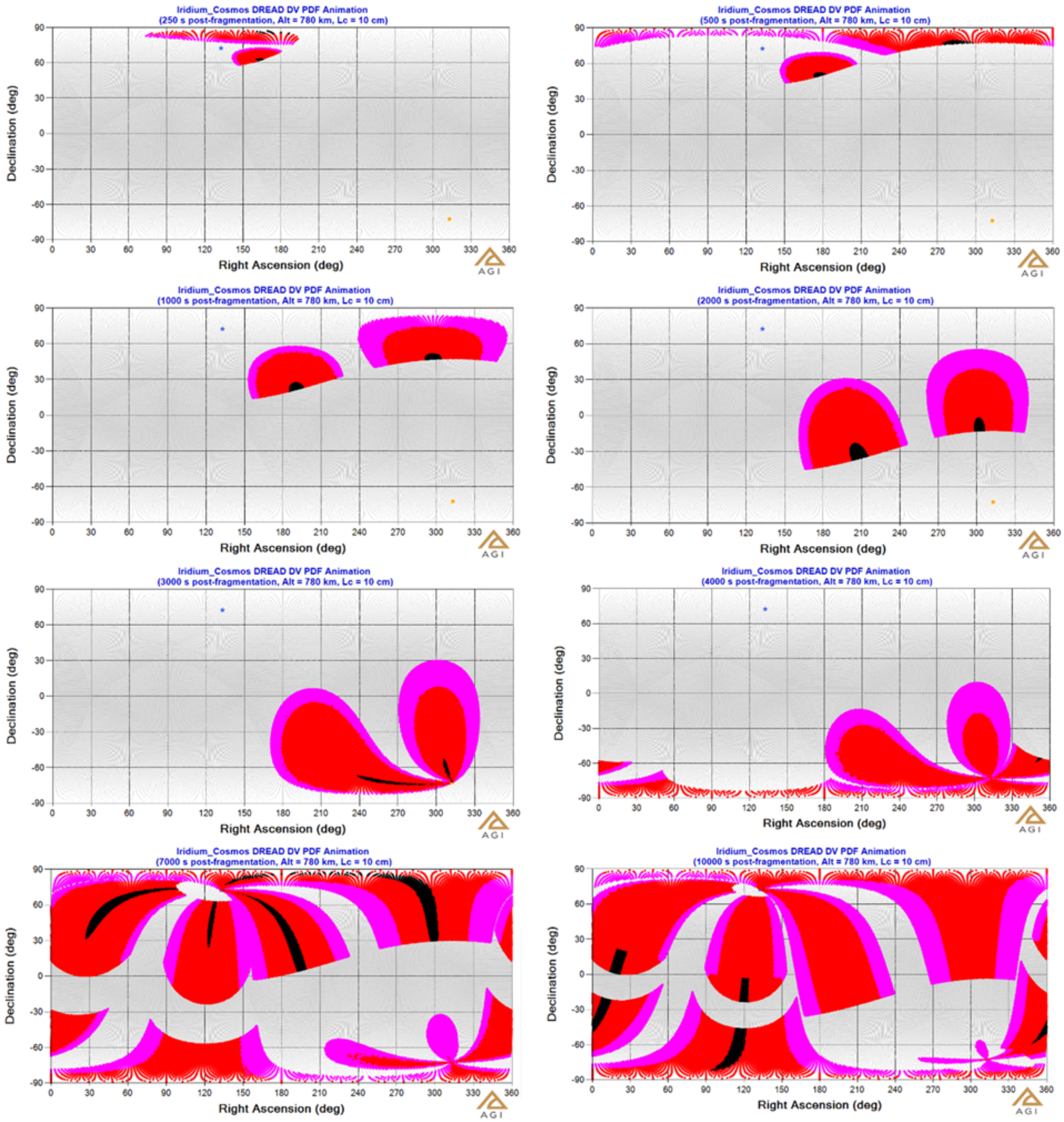

Figures 17: LEO Debris Location over Time. The likelihood that an Iridium/Cosmos fragment will acquire Δv necessary to be located at any Right Ascension-Declination points at a later specified time. As time progresses, many more locations "may" contain debris.

Note that the locus of points (and volume) where fragments might exist as a function of time encompasses an area much larger than a simple region around the two initial velocity directions. Also keep in mind that these 2D images represent an "altitude slice" and that fragments may be located well-outside the depicted regions at other altitudes than that of the fragmentation event.

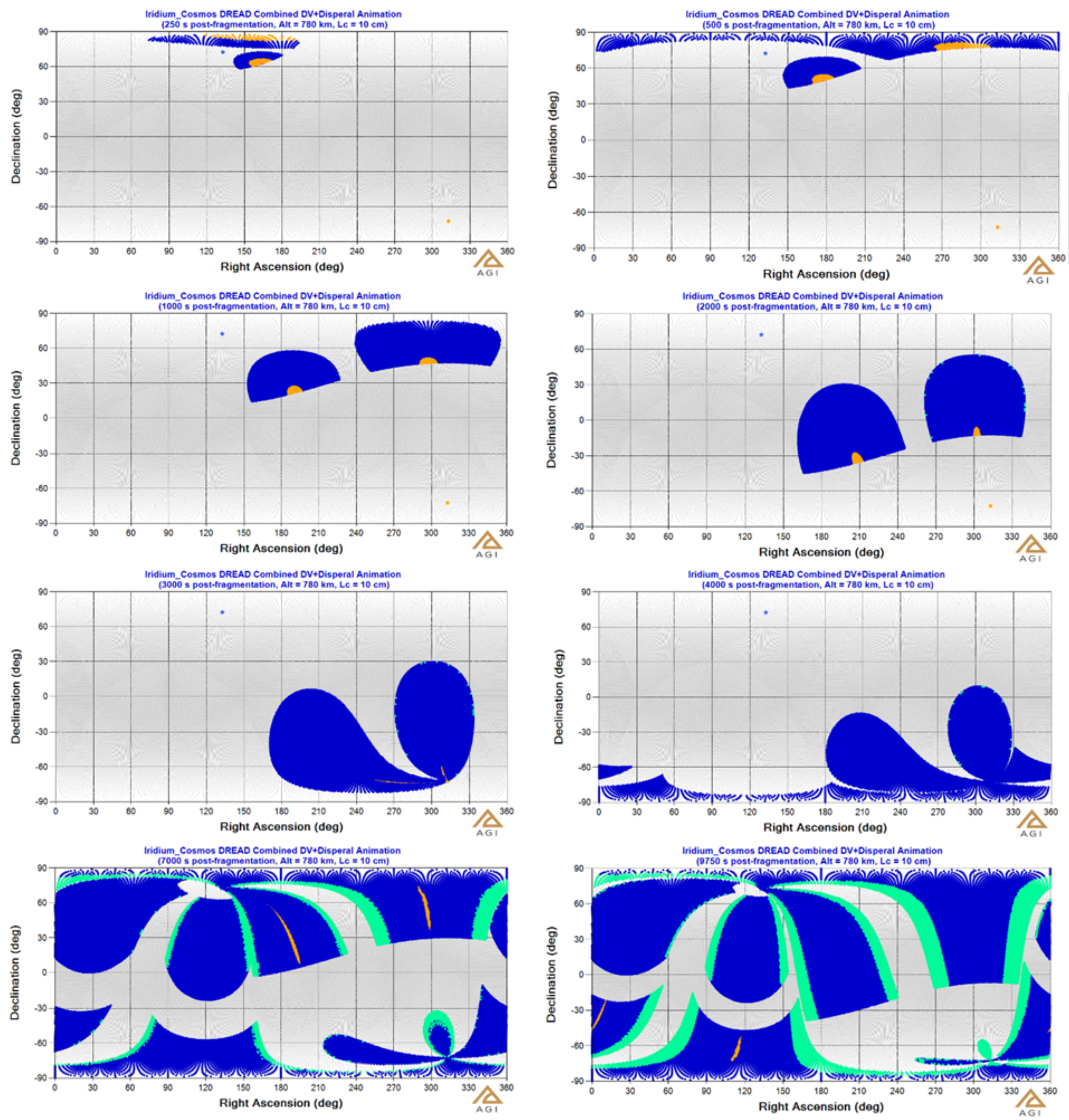

Figures 18: LEO Debris Location over Time. The likelihood that an Iridium/Cosmos fragment will acquire Δv necessary to be located at any Right Ascension-Declination points at a later specified time combined with the likelihood that a particle will be in a space "voxel" of interest.

In the above figures, the reader will note that the overall shapes are identical to the previous set of plots, but now the likelihood numbers are further de-weighted by the volume of space that the fragmentation cloud occupies at any given time; i.e., as a fixed number of fragments disperse into different altitudes and locations within an altitude shell, the likelihood of a fragment being in a "voxel of space" at a given time falls proportionally to the volume of space occupied by the fragmentation cloud.

Upon completion of the simulation, an aggregate depiction of the inertial space that debris fragments could occupy during the simulation time span (0 to 10,000 seconds) can be created as shown below. The "saw tooth" nature of the densest regions is simply an artefact of the coarse time step used in this sample case.

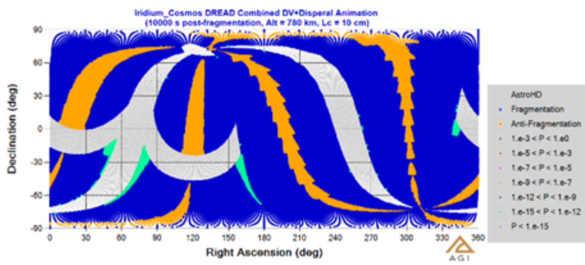

Figure 19: Aggregate Results. The likelihood that an Iridium/Cosmos fragment will acquire Δv necessary to be located at any Right Ascension-Declination points at a later specified time combined with the likelihood that a particle will be in a space "voxel" of interest.

Plotting the dispersal volume shows that the volume increases over time, but not at a uniform rate. The pinch points are seen as reductions in the dispersal volume, and the non-smooth nature of the plot is due to fragments traveling at different orbital speeds. In the DREAD tool, this volumetric expansion is used to de-weight the likelihood as mentioned above. Note, however, that in these two sample LEO and GEO cases, our grid was not of sufficient depth and resolution to yield an absolute weighting. Rather, our sample results should be viewed as fairly accurate in a relative sense.

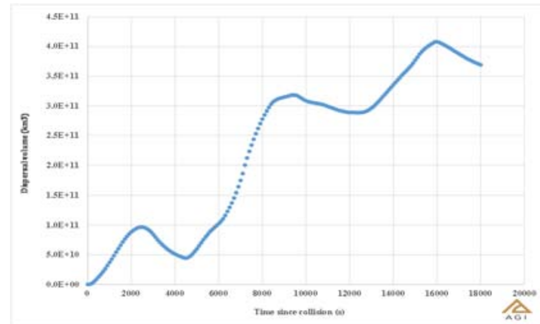

Figure 20: Iridium/Cosmos Accessible Dispersal Volume. The debris fragments encompasses a generally increasing volume over time. However, as individual fragments reach pinch points at different times, the volume experiences corresponding contractions.

12. EXAMINATION OF A HYPOTHETICAL GEO COLLISION

For the GEO simulation, we examined a hypothetical collision between an active equatorial GEO satellite and a GEO space debris object inclined at 15 degrees (relative velocity of 805 m/s at impact). The assumed geometry is shown below.

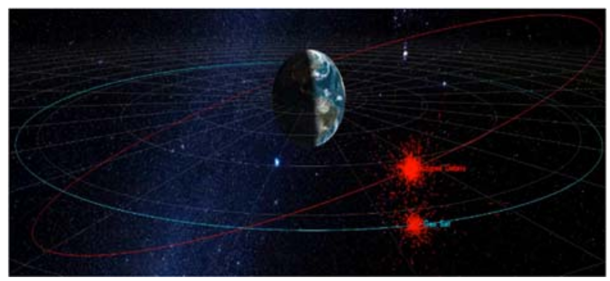

Figure 21: Hypothetical GEO Collision Case. A hypothetical low velocity collision in GEO is shown shortly after impact.

This hypothetical GEO collision case is decidedly below the threshold of what could be considered a "hypervelocity impact" but at the same time, 805 m/s will certainly lead not only to plastic deformation but also to major destruction and resulting fragmentation. For this case, we utilized the relatively simple NASA Standard Breakup Model modifications for low-velocity collisions indicated by the small body of research conducted by Hanada, 2000.

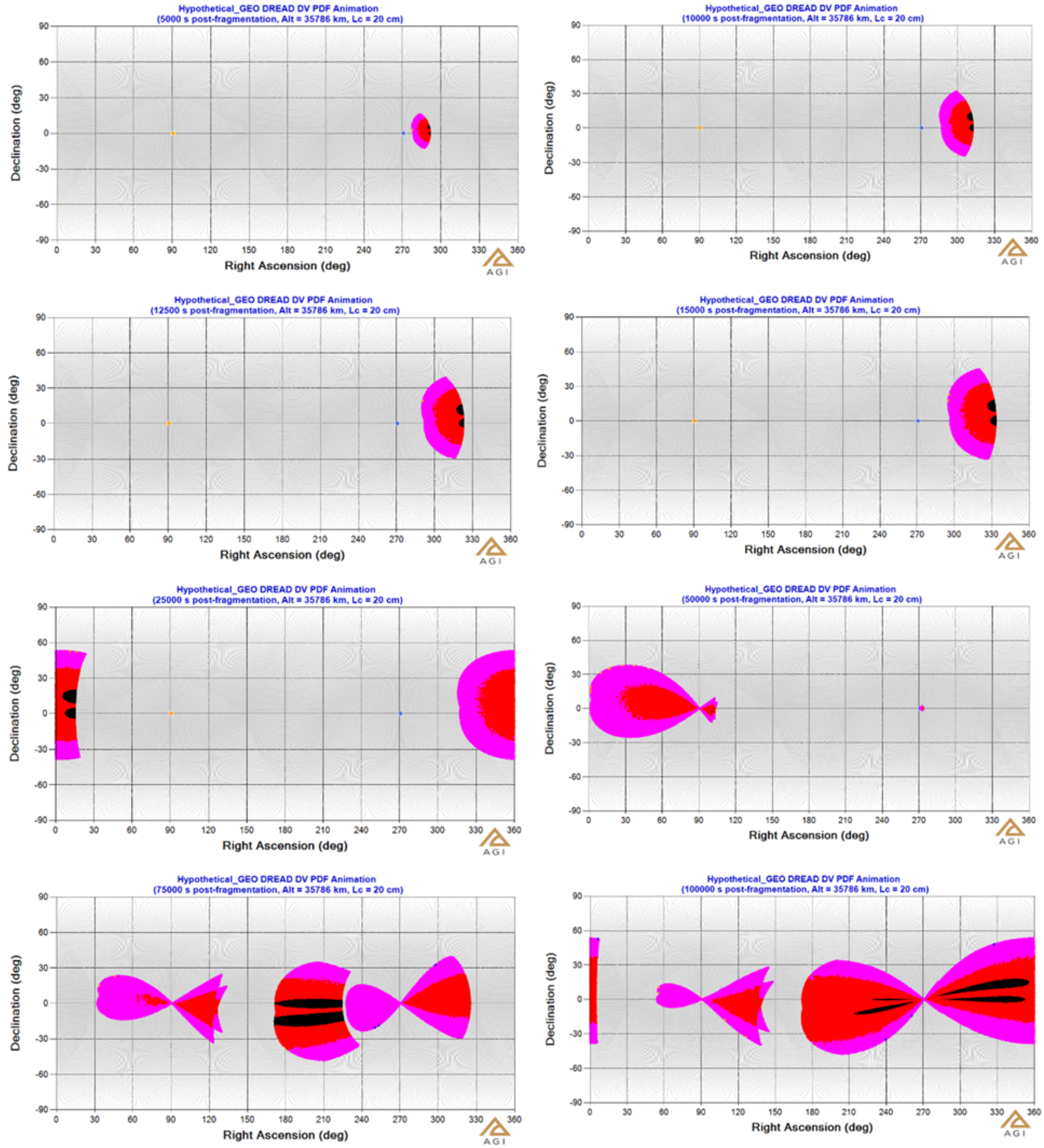

Figures 22: GEO Debris Location over Time. The likelihood that a fragment from the hypothetical GEO collision case will acquire Δv necessary to be located at any <u>inertial</u> Right Ascension-Declination points at a later specified time combined with the likelihood that a particle will be in a space "voxel" of interest.

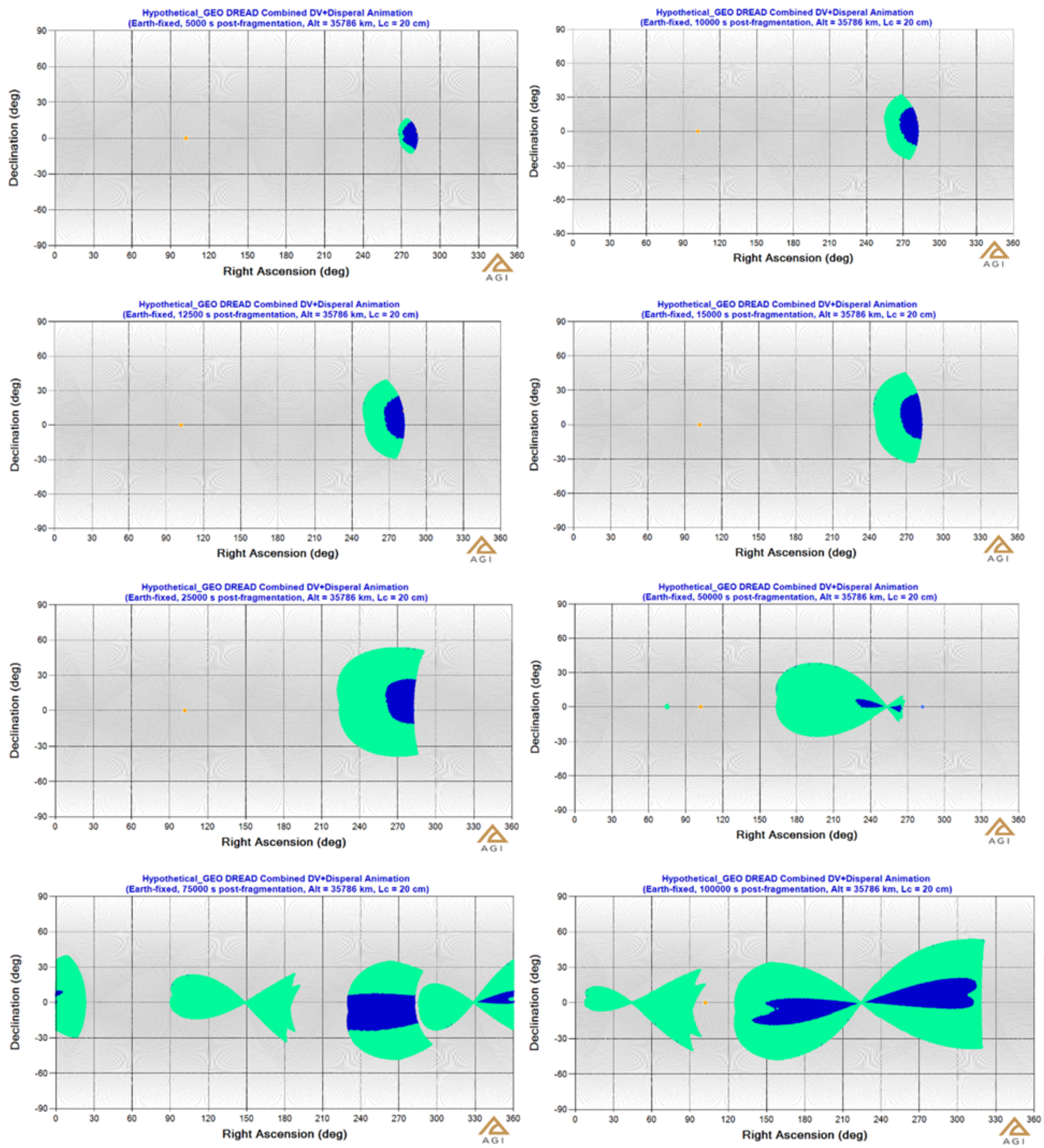

Figures 23: GEO Debris Location over Time. The likelihood that a fragment from our hypothetical GEO collision case will acquire Δv necessary to be located at any Earth-Fixed Longitude - Latitude points at a later specified time combined with the likelihood that a particle will be in a space "voxel" of interest.

13. ASSESSING SATELLITES AT RISK

A concern we have had is that fragments may not all be depicted in discrete fragment simulations, and resulting satellite collisions may not adequately depict the risk over time. This new analysis capability is well-suited for identifying active satellites placed in harm's way by a collision or explosion event. The risk posed to the satellites can be assessed in a relative sense, allowing rank-ordering of risk, notification to the operators flying those satellites, and identification of when and where the greatest relative risk will occur. As an example, the top 20 satellites at greatest risk for the LEO and GEO scenarios are provided below.

Table 2: LEO Iridium/Cosmos collision "Top 20" active satellites placed at greatest risk.

SSC	Intl Desig	Risk to S/C
22490	SCD 1	7.32E-07
24949	IRIDIUM 30	3.06E-07
25274	IRIDIUM 58	2.51E-07
25475	ORBCOMM FM21	2.05E-07
24869	IRIDIUM 15	2.02E-07
15427	NOAA 9	1.87E-07
27375	IRIDIUM 95	1.76E-07
27374	IRIDIUM 94	1.72E-07
24950	IRIDIUM 31	1.53E-07
25272	IRIDIUM 55	1.38E-07
25414	ORBCOMM FM18	1.35E-07
31118	SAUDISAT 3	1.28E-07
27372	IRIDIUM 91	1.21E-07
25275	IRIDIUM 59	1.17E-07
31124	SAUDICOMSAT 5	1.03E-07
24795	IRIDIUM 5	1.01E-07
25117	ORBCOMM FM05	1.01E-07
29499	METOP-A	9.66E-08
25276	IRIDIUM 60	9.06E-08
33321	HUANJING 1B (HJ-1B)	7.03E-08

Table 3: GEO hypothetical collision "Top 20" active satellites placed at greatest risk.

SSC	Intl Desig	Risk to S/C
22490	SCD 1	7.32E-07
24949	IRIDIUM 30	3.06E-07
25274	IRIDIUM 58	2.51E-07
25475	ORBCOMM FM21	2.05E-07
24869	IRIDIUM 15	2.02E-07
15427	NOAA 9	1.87E-07
27375	IRIDIUM 95	1.76E-07
27374	IRIDIUM 94	1.72E-07
24950	IRIDIUM 31	1.53E-07
25272	IRIDIUM 55	1.38E-07
25414	ORBCOMM FM18	1.35E-07
31118	SAUDISAT 3	1.28E-07
27372	IRIDIUM 91	1.21E-07
25275	IRIDIUM 59	1.17E-07
31124	SAUDICOMSAT 5	1.03E-07
24795	IRIDIUM 5	1.01E-07
25117	ORBCOMM FM05	1.01E-07
29499	METOP-A	9.66E-08
25276	IRIDIUM 60	9.06E-08
33321	HUANJING 1B (HJ-1B)	7.03E-08

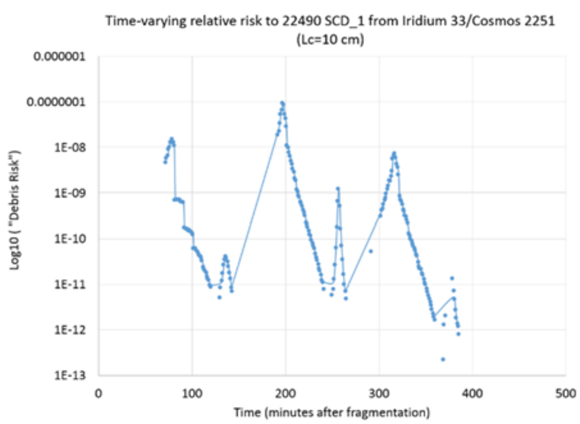

Figure 24: DREAD-estimated time history of debris risk by LEO Iridium/Cosmos to active satellite w/greatest risk.

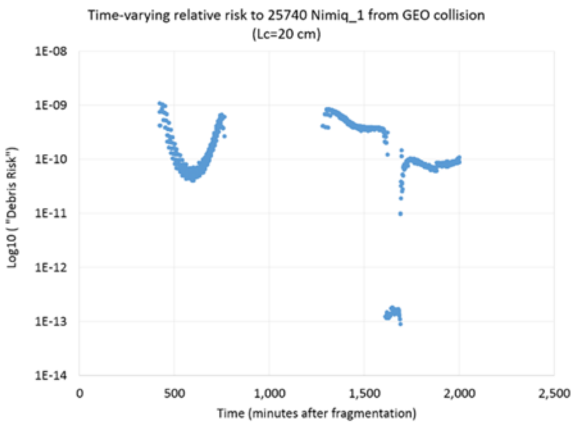

Figure 25 DREAD-estimated time history of debris risk by GEO collision to active satellite w/greatest risk.

14. CONCLUSIONS

Visualizing debris cloud evolution in 3D was a challenging task, and a computationally expensive operation. Nevertheless, we arrived at a solution combining many separate programs, and can make detailed runs in a day or so on a laptop. More importantly, we found that using a grid approach, we could sample spaces that may have never been fully explored. We also observed much larger regions where debris fragments could potentially exist because we sampled all of space, rather than starting from discrete initial velocity values.

As expected, the majority of the fragments are located within two general orbital cloud regions. However, we found that additional objects were dispersed at much larger distances than generally shown in existing analyses. This has direct implications for collision risk calculations.

We encourage the research community to develop better breakup models. There are new materials not reflected in the NASA standard breakup model. In addition, lower velocity impacts (below hypervelocity) could be useful to extend the analysis to orbital regimes where closing velocities are smaller.

15. FUTURE WORK

Merging multiple programs together proved a challenge! There are several things we would like to investigate further. Additional approaches are likely useful for more accurately finding the 180° transfer cases. (Thompson, 2011)

We are also planning to use the new DREAD tool to explore and characterize fragmentation debris dispersal for a host of historical and hypothetical (future) collision and explosion cases.

It is also of great interest to us to employ other breakup, hypervelocity and low velocity fragmentation models to better adhere to physical conservation laws, incorporate/address current S/C materials properties and draw upon any new, detailed hypervelocity impact code/simulations.

Finally, we wish to investigate incorporation of secular and potentially short-periodic perturbations to improve the accuracy of the solutions over longer periods of time.

16. ACKNOWLEDGEMENT

We want to acknowledge the contributions of Scott Reynolds to our volumetric depiction development work.

17. REFERENCES

Alfano, Salvatore, and Daniel Oltrogge. 2015. Volumetric Encounter Analysis Enhancements. Paper AAS 15-581 presented at the AAS/AIAA Astrodynamics Specialist Conference. Vail, CO.

Arora, Nitin and Ryan P. Russell. 2013 A Fast and Robust Multiple Revolution Lambert Algorithm Using a Cosine Transformation. Paper AAS 13-728 presented at the AAS/AIAA Astrodynamics Specialist Conference. Hilton Head, SC.

Carrico, Timothy and John Carrico. 2008. Investigating Orbital Debris Events using Numerical Methods with Full Force Model Orbit Propagation. Paper AAS 08-126 presented at the AAS/AIAA Spaceflight Mechanics Conference, January 28-31. Galveston, TX.

Chobotov, V. A., et al. 1988. Dynamics of Debris Motion and the Collision Hazard to Spacecraft Resulting from an Orbital Breakup. Aerospace Report SD TR-88-96, Space Division AFSC. Los Angeles, CA.

Finkleman, David, Daniel L. Oltrogge, Anthony Faulds, and Joseph Gerber. 2008. Analysis of the Response of a Space Surveillance Network to Orbital Debris Events. Paper AAS 08-127 presented at the AAS/AIAA Spaceflight Mechanics Conference, January 28-31. Galveston, TX.

Gabbard, J. R. 1981. The Explosion of Satellite 10704 and Other Delta Second Stage Rockets. Technical Memorandum 81-5. Directorate of Analysis NORAD/ADCOM. May 1981.

Hanada, Toshiya. 2000. Developing a Low-Velocity Collision Model Based on the NASA Standard Breakup Model. *Space Debris*. 2:4, pp.233-247.

Healy, Liam, et al. 2016. Spatial Density maps from a

Debris Cloud. Paper presented at the AMOS Advanced Maui Optical and Space Surveillance Technologies Conference. Maui, HI. September 20-23.

Houlton B., and D. Oltrogge. 2014. Commercial Space Operations Center (ComSpOC): A Commercial Alternative for Space Situational Awareness (SSA). Paper presented at the 30th Space Symposium Tech Track. Colorado Springs, CO.

Hujsak, Richard S. 1991. Nonlinear dynamical model of relative motion for the orbiting debris problem. *Journal of Guidance, Control, and Dynamics.* 14.2, pp. 460-465.

Johnson, N. L. et al. 2001. NASA's new breakup model of evolve 4.0. *Advances in Space Research.* 28.9, pp. 1377-1384.

Johnson, Nicholas L. 2008. History of on-orbit satellite fragmentations 14th Ed. NASA TM 2008 214779.

McKennon-Kelly, Ryan et al. 2015. Seeing Through the Clutter: The Power of the Torus. Aerospace Crosslink 16:1. Pp. 40-45.

Oltrogge, Dan. 2008. Breakup Modeling with 1Earth's DebBIE Module and STK. Paper AGI-UTH-Oltrogge presented at the AGI Users Conference, October 7-9. Chicago, IL.

Oltrogge, Daniel L. 2008. AstroHD™: Astrodynamics Modeling with a Distinctly Digital Flavor. Paper AIAA 2008-7065 presented at the AAS/AIAA Astrodynamics Specialist Conference, August 18-21. Honolulu, HI.

Thompson, Blair F. 2011. Enhancing Lambert Targeting Methods to Accommodate 180-Degree Orbital Transfers. *Journal of Guidance, Control, and Dynamics.* 34.6, pp. 1925-1928.

Vallado, David A. 2013. *Fundamentals of Astrodynamics and Applications*. Fourth Edition. Microcosm, Hawthorne, CA